COMPUTATIONAL FLUID DYNAMICS APPLICATIONS AT MCDONNELL DOUGLAS

R. J. Hakkinen*

McDonnell Douglas Research Laboratories

SUMMARY

Representative examples are presented of applications and development of advanced Computational Fluid Dynamics (CFD) codes for aerodynamic design at the McDonnell Douglas Corporation (MDC). Transonic potential and Euler codes, interactively coupled with boundary layer computation, and solutions of slender-layer Navier-Stokes approximation are applied to aircraft wing/body calculations. An optimization procedure using evolution theory is described in the context of transonic wing design. Euler methods are presented for analysis of hypersonic configurations, and helicopter rotors in hover and forward flight. Several of these projects have been accepted for access to the Numerical Aerodynamic Simulation (NAS) facility at the NASA-Ames Research Center.

1. INTRODUCTION

Computational fluid dynamics (CFD) is used as a routine design technique in the divisional engineering technology and project organizations of the McDonnell Douglas Corporation (MDC). Several groups are also active in research and development of CFD methods, both at the divisional companies in the context of their primary applications, and in a more generic sense at the McDonnell Douglas Research Laboratories (MDRL). Figure 1 shows a simplified corporate organization chart.

In addition to the computing facilities at divisional locations, a Cray X-MP/14 is available as a central resource under the management of the McDonnell Douglas Aerospace Information Services Company. When authorized, U. S. Government large-scale computing facilities are used for specific tasks; cooperative projects with NASA centers have been especially fruitful.

The following examples describe CFD applications to aerodynamic design and optimization, and new methods under development for computation of aircraft, helicopter, and missile flowfields. These projects are supported by the McDonnell Douglas Corporation Independent Research and Development Program; for several projects, the cooperation of the NASA NAS Program and/or of Cray Research, Inc., is appreciated.

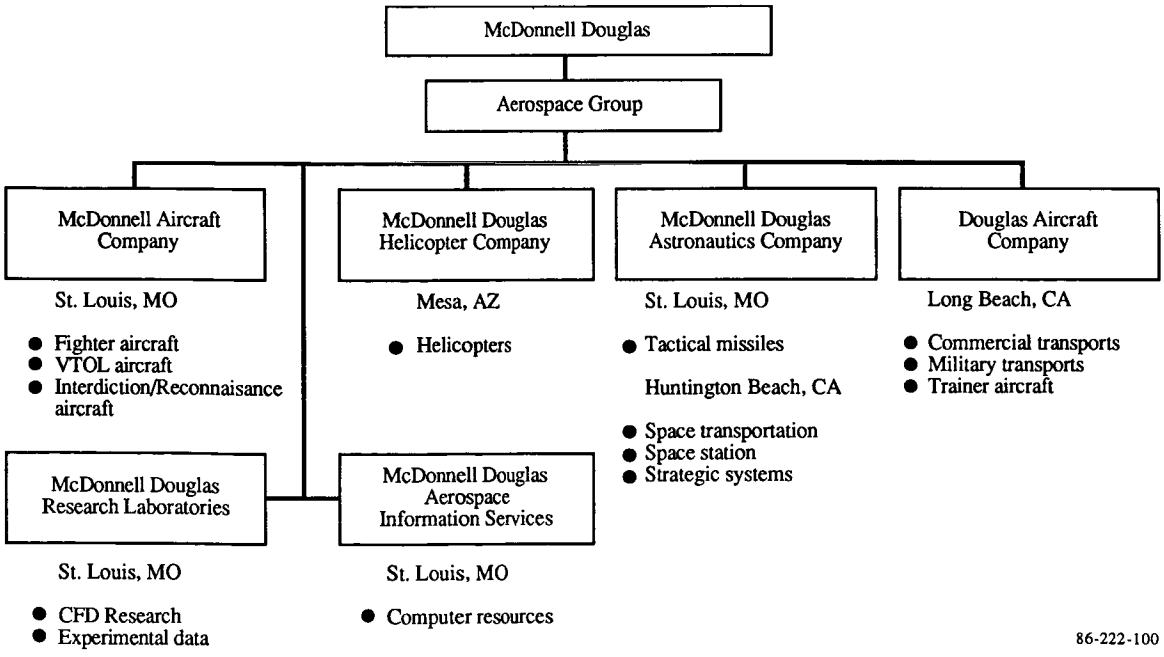

Fig. 1 McDonnell Douglas Aerospace Group components active in CFD.

*Director-Research, Flight Sciences Department.

2. **Simulation of Power Effects on Complex Configurations with an Inviscid/Viscous Interaction Scheme Based on the Solution of Euler and Inverse Boundary Layer Equations** (T. Cebeci and L. T. Chen, Douglas Aircraft Company (DAC), Long Beach, CA)

The objective of this project (fig. 2) is to combine transonic flowfield codes based on the Euler equations with a three-dimensional inverse boundary-layer method. Complex wing/body and aft fuselage/nacelle/pylon configurations, including power effects, will be computed with different grid topologies. The results will be compared with available experimental data. The computer resources used in this project include the NAS Cray-2.

Successful computation of flows with both shock-induced and trailing-edge separation requires the combination of viscous/inviscid interactive schemes with the Euler equations which provide a realistic simulation of the vorticity distribution downstream of strong shocks. In the inverse boundary-layer method of Cebeci, et al. (1986), the edge velocity is treated as an unknown and the interactive solutions are obtained with the Hilbert integral approach. The coupling of the inverse method with two-dimensional Euler equations is presented by Chen, Li and Chen (1987); Chen and Chen* extend this approach to three dimensional transonic flows over wings and wing/body configurations.

The computational procedure of Chen and Chen* also extends the hybrid mapping/numerical grid-generation method of Chen, Vassberg and Peavey (1985) to a new scheme where the mesh lines are wrapped around the wing tip into a C-mesh which allows proper modeling of wing-tip vorticity permitted by the Euler equations, as shown in figure 3.

Task 1:	Develop and validate Euler methods for wing/body and aft-fuselage/nacelle/pylon configurations, respectively, on NAS computer.
Task 2:	Develop and validate an interactive inverse boundary-layer method for coupling with the Euler method wing/body and aft-fuselage/nacelle/pylon configurations, respectively.
Tack 3:	Validate solutions for both configurations on the NAS computer for a wide range of flow conditions and power settings, and study the mesh effect on the solutions by comparing them with DAC full-potential and Euler-correction solutions.
Task 4:	Develop a zonal method for coupling solutions about wing/body and aft-fuselage/nacelle/pylon configurations.
Task 5:	Compare computed solutions with available test data.

GP61-1439-2-R

Fig. 2 Simulation of power effects on complex configurations with an inviscid/viscid interaction scheme based on the solution of Euler and inverse boundary-layer equations.

*Chen, L. T. and Chen, H., "An Interactive Scheme for Transonic Wing/Body Flows Based on Euler and Inverse Boundary-Layer Equations," Douglas Aircraft Company, Long Beach, CA, 1987.

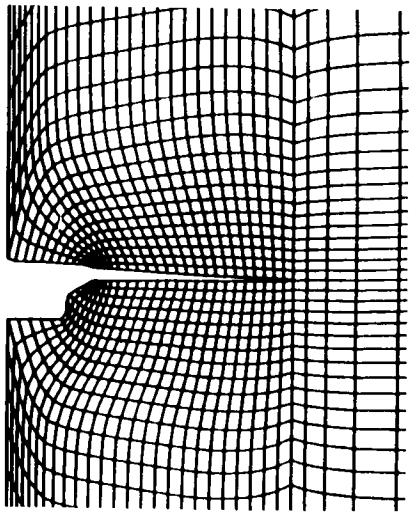

(a) KGRID (C-H-H mesh)

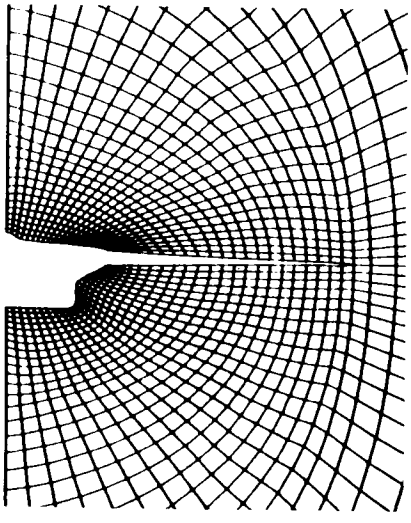

(b) PGRID (C-C-H mesh)

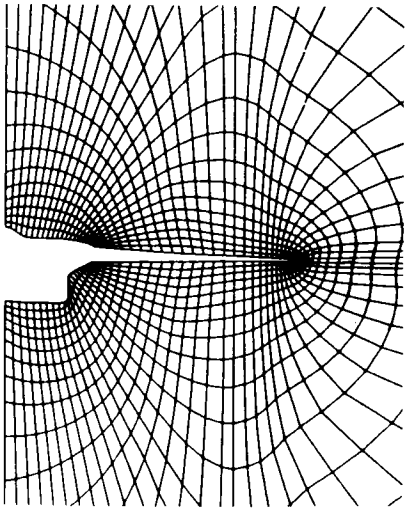

(c) QGRID (C-C-C mesh)

GP61-1439-3-R

Fig. 3 Comparison of cross-sectional grid distribution for three grid-generation methods.

The three-dimensional inviscid flowfield is calculated with Jameson's multi-grid, four-stage Runge-Kutta time-stepping scheme, and the inverse boundary-layer method of Cebeci et al. (1986) is applied with a strip theory approximation. Both displacement surface and blowing velocity approaches are used in the interactive matching procedure described in detail by Chen and Chen.*

Figure 4 shows an inviscid Euler calculation of supersonic flow about a fighter-type wing/fuselage configuration. The calculation was obtained with the new grid-generation method described by Chen, Vassberg, and Peavey (1985) and Chen and Chen.* A comparison of viscous/inviscid interactive calculations with test data is shown in figure 5 for a high-aspect-ratio transport wing/body configuration. Both potential and Euler codes were used for the inviscid flowfield, and the interactive coupling was accomplished by the displacement surface approach. The agreement between the calculations and experiment is generally good, with some deterioration toward the wing tip.

Further improvements of the grid-generation method will include implementation of the zonal technique for complex configurations.

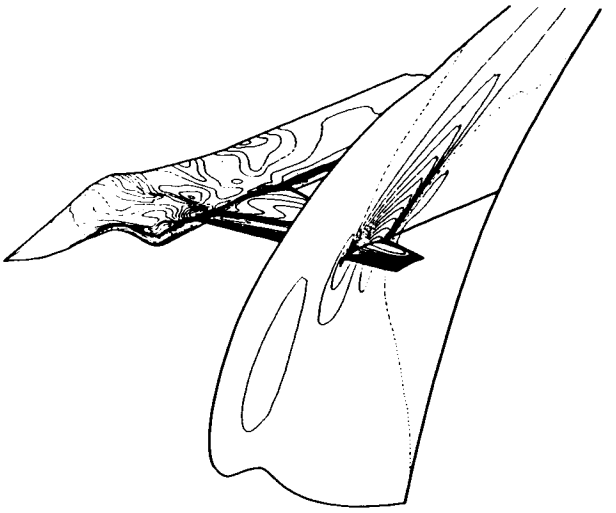

Fig. 4 Mach number contours on a typical fighter wing/fuselage; $M_\infty = 1.3$ and $\alpha = 4.84°$.

3. Transonic Wing Optimization By Evolution Theory (R. D. Gregg, Douglas Aircraft Company, Long Beach, CA)

The present comments are based on Gregg and Misegades (1987), which contains a more extensive discussion of the impact of increasing computer capability on three-dimensional optimization procedures and presents detailed practical results.

The importance of computing speed is illustrated in figure 6, where the assumption of an optimization process requiring 1000 transonic wing flowfield solutions indicates the dramatic effect of computational speed: the approximately 250 hours required by an IBM 3081 can be reduced to ten hours on a single-processor Cray X-MP, and to 2.5 hours when taking full advantage of the multitasking capability of a Cray X-MP/48.

A description of the evolution-theory approach is shown in figure 7. Basically, a set of merit functions related to performance requirements is calculated repeatedly for different sets of design variables that are allowed to vary within a chosen range. At each step, the range and its center are adjusted until a reasonable convergence of the merit functions is achieved.

Figure 8 illustrates how the convergence of merit functions was achieved in the case of an aspect ratio of ten, taper ratio of four, 25-degree swept NACA 0012 wing which was allowed to change camber in the last 15 per cent of chord. The flight condition was M=0.76 at C_L=0.55, and the base wing exhibited excessive shock drag, buffet, and tip stall. While induced drag increased slightly because of increased departure from an elliptic spanwise load distribution, significant gains in other merit functions were achieved in approximately forty iterations, including a 50-per cent decrease in total drag.

The procedure involved 640 FLO-22 solutions with a total CPU-time of 7.2 hours. This example is the first one of three in this paper where the microtasking procedure of Booth and Misegades (1986) was used in cooperation with Cray Research on their Cray X-MP/48, resulting in this case in clock-time reduction by a factor of 3.95 to 1.8 hours.

4. Accurate, Efficient Prediction Method for Supersonic/Hypersonic Inviscid Flow (A. Verhoff and P. J. O'Neil, McDonnell Aircraft Company, St. Louis, MO)

The new method employs a spatial marching procedure to solve the formulation of Euler equations described by Verhoff and O'Neil (1984). This formulation is written in terms of Riemann-type variables by use of a local streamline coordinate system shown in figure 9, and therefore models wave propagation in a physical sense with no inherent Mach-number restrictions. The procedure can be extended to three-dimensional flows in a straightforward manner, and it is especially suitable for efficient vector coding.

Steady-state solutions are obtained by an explicit time-integration scheme, where the local maximum time step is used to increase rate of convergence. Spatial derivatives are approximated by one-sided finite differences to properly model the wave propagation. At solid surfaces, the algebraic relationship between the flow angles θ and ϕ, combined with the local pressure gradient, yields an accurate boundary condition. Neither non-physical

*Chen, L. T. and Chen, H., "An Interactive Scheme for Transonic Wing/Body Flows Based on Euler and Inverse Boundary-Layer Equations," Douglas Aircraft Company, Long Beach, CA, 1987.

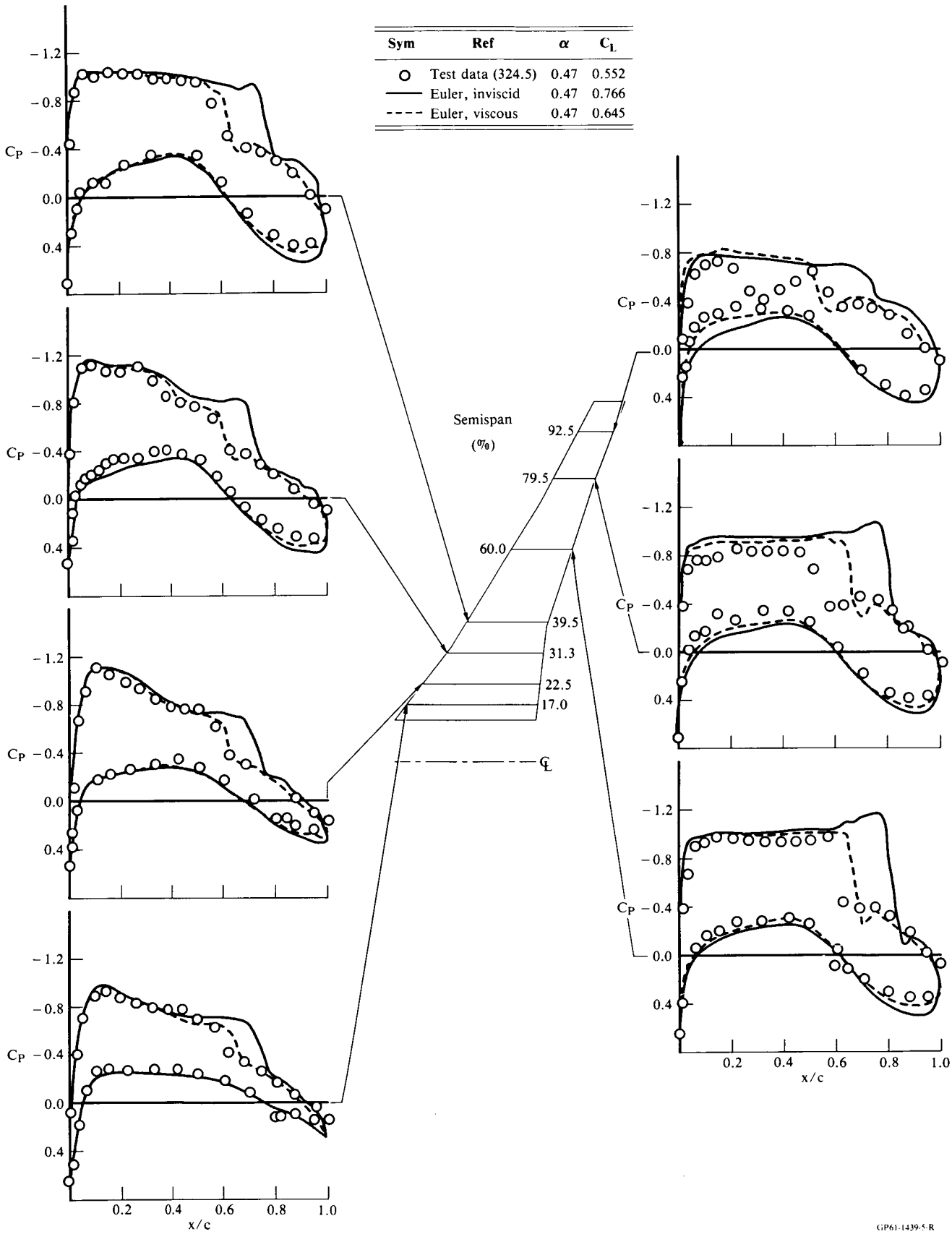

Fig. 5 Comparison of viscous/inviscid Euler solutions and test data for the LB-488 wing/body; $M = 0.82$, $\alpha = 0.47$; and $Re_c = 5.4 \times 10^6$.

input parameters, artificial dissipation, nor smoothing are required in the solution algorithm.

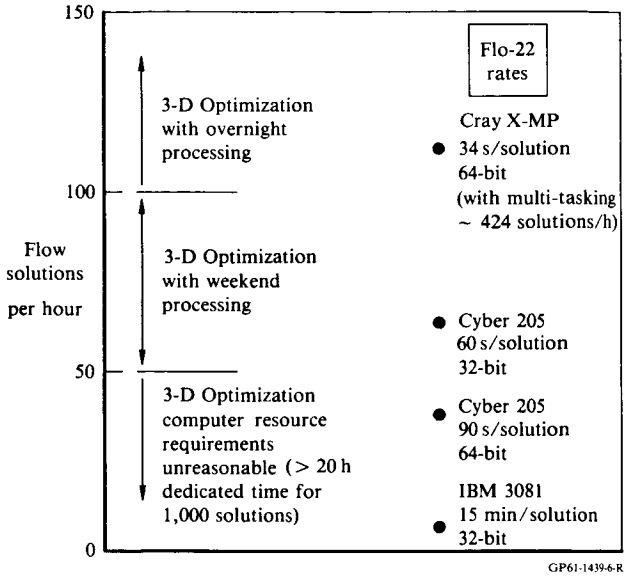

Fig. 6 Aerodynamic wing optimization: the importance of computational speed.

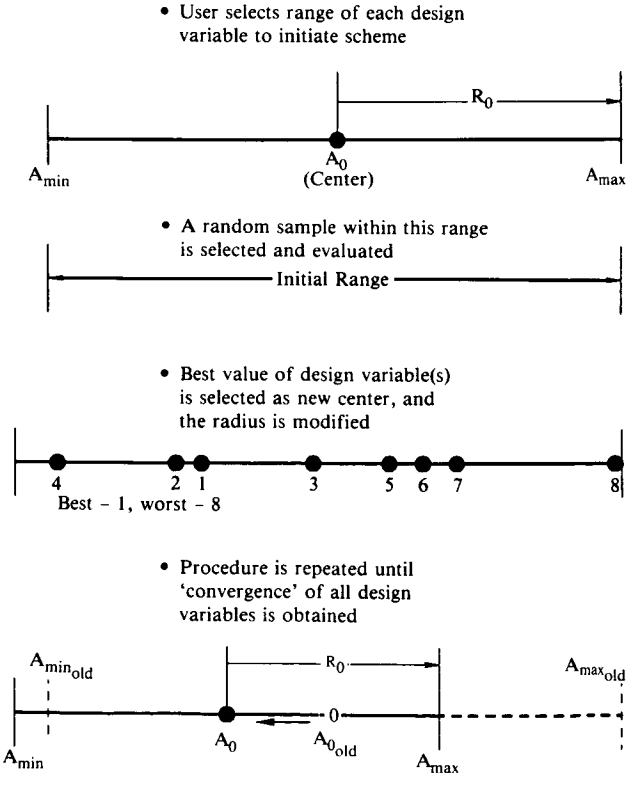

Fig. 7 Evolution theory.

For fully inviscid supersonic flow, three-dimensional flowfield analysis can be reduced to a sequence of two-dimensional problems by use of a spatial marching procedure based on this formulation. Flowfields about vehicles with wings, tails, and fins can therefore be predicted with relatively coarse computational grids. Shocks are automatically captured; the only constraint requires the outer grid boundary to include the perturbed flowfield.

A computer program called SCRAM (Streamline Coordinate Riemann Axial Marching) has been developed at McDonnell Aircraft using this formulation. The program evolved from a research code and within one year became a useful design method for routine analysis of hypersonic configurations. A detailed description of the method is presented by Verhoff and O'Neil,* including the following representative examples.

Figure 10 illustrates the suitability of the SCRAM-code for vector processing in the case of a simple 20-degree cone at zero angle of attack in

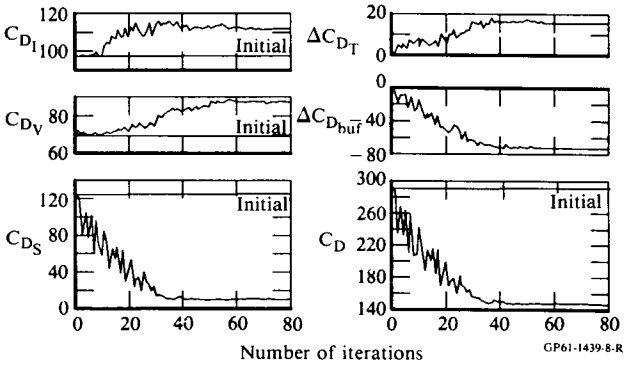

Fig. 8 Aerodynamic wing optimization for a simple, swept-wing test case (in terms of induced, viscous, shock, trim, buffet, and total drag).

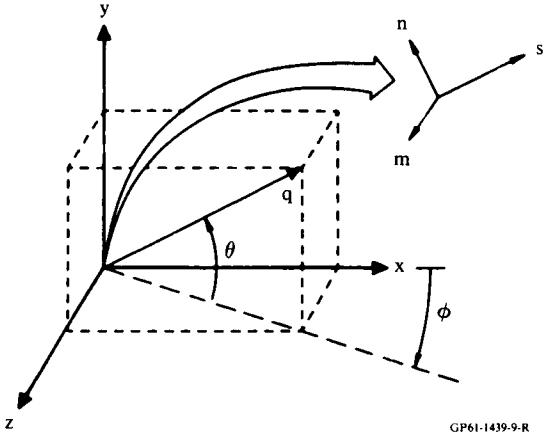

Fig. 9 Definition of flow angles and streamline coordinates.

*Verhoff, A. and O'Neil, P. J., "Accurate, Efficient Prediction Method for Supersonic/Hypersonic Inviscid Flow," McDonnell Aircraft Company, St. Louis, MO, 1987.

M=2.5 supersonic flow; CPU time reductions by an order of magnitude can be achieved for higher grid densities relative to scalar operation. Figure 11 shows the accuracy of the solution for various grid densities, as compared with the exact analytical solution.

Figure 12 shows the computational grid for a blended wing/body configuration. The grid has half-plane distribution of 51 by 25 nodes, with 25 axial stations, and is based on a nonlinear grid generation procedure developed at McDonnell Aircraft. For M=6, computed pressure contours in four cross-planes are shown in figure 13, and a comparison of predicted force and moment characteristics with test data is shown in figure 14; estimated skin-friction drag has been subtracted from the test data, yielding excellent agreement with the inviscid computation. Each case, including input-output processing, required only about five minutes on the Cray X-MP/14.

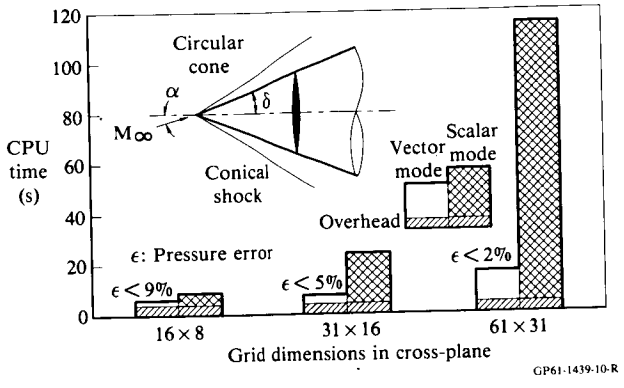

Fig. 10 Vector efficiency of SCRAM code on CYBER 205 computer; $M_\infty = 2.5$, $\delta = 20°$, and $\alpha = 0°$.

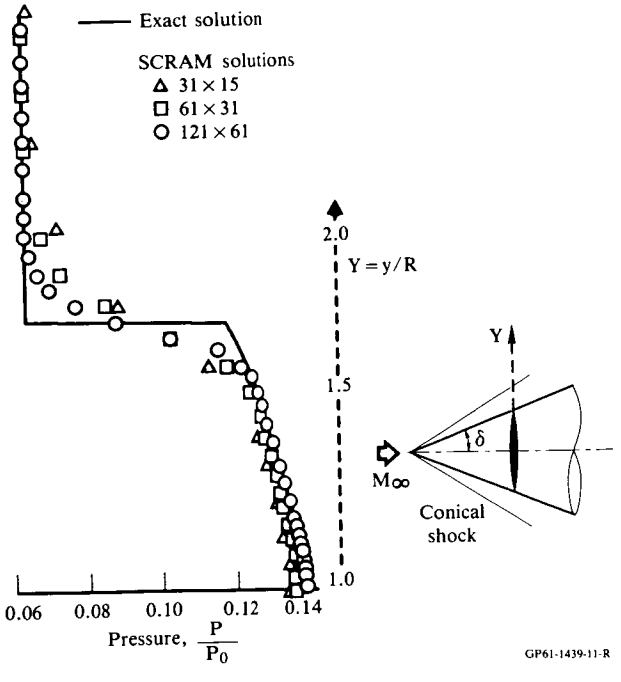

Fig. 11 SCRAM solution for circular cone; $M_\infty = 2.44$, $\alpha = 0°$, and $\delta = 20°$.

Figures 15 and 16 show the grid and the computed Mach number contours, respectively, for a complex conical body at M=10. The excellent grid resolution and computational efficiency contributed to the achievement of a converged solution at the first attempt, again requiring approximately five minutes on the Cray X-MP/14.

McDonnell Aircraft is applying the SCRAM code to high-quality prediction of increasingly complex flowfields, including realistic fighter and hypersonic aircraft configurations.

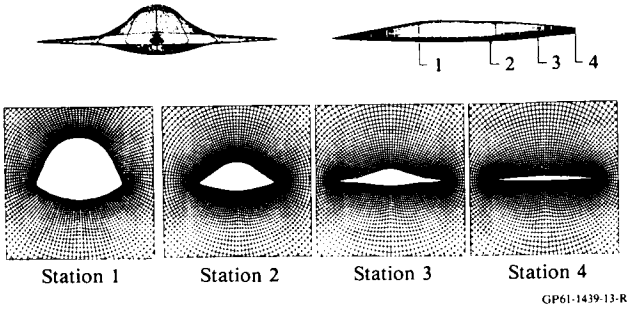

Fig. 12 Computational grid for AMI-X blended body; vertical tails off.

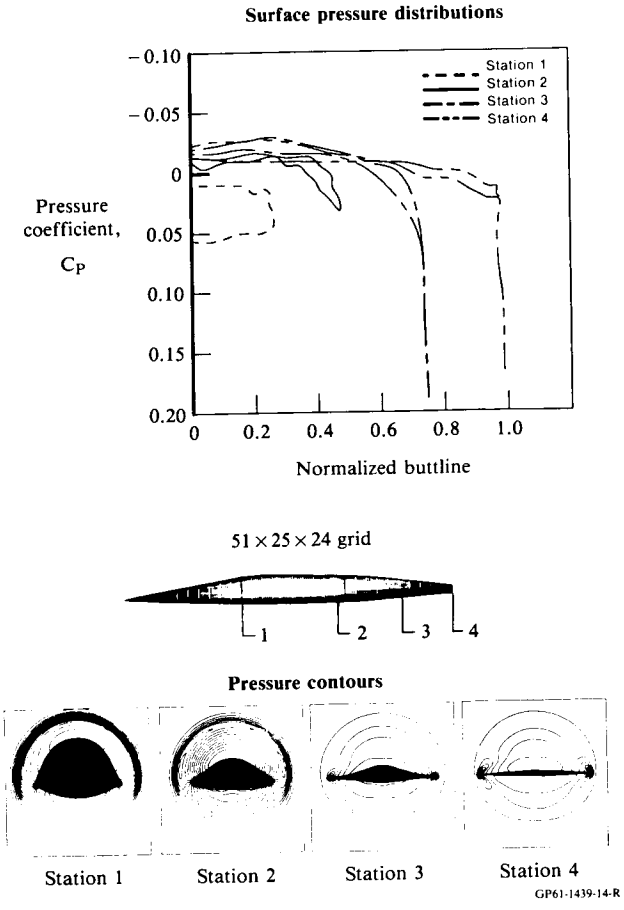

Fig. 13 SCRAM pressure predictions for AMI-X blended body; $M_\infty = 6$ and $\delta = 0°$.

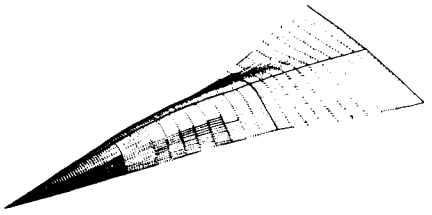

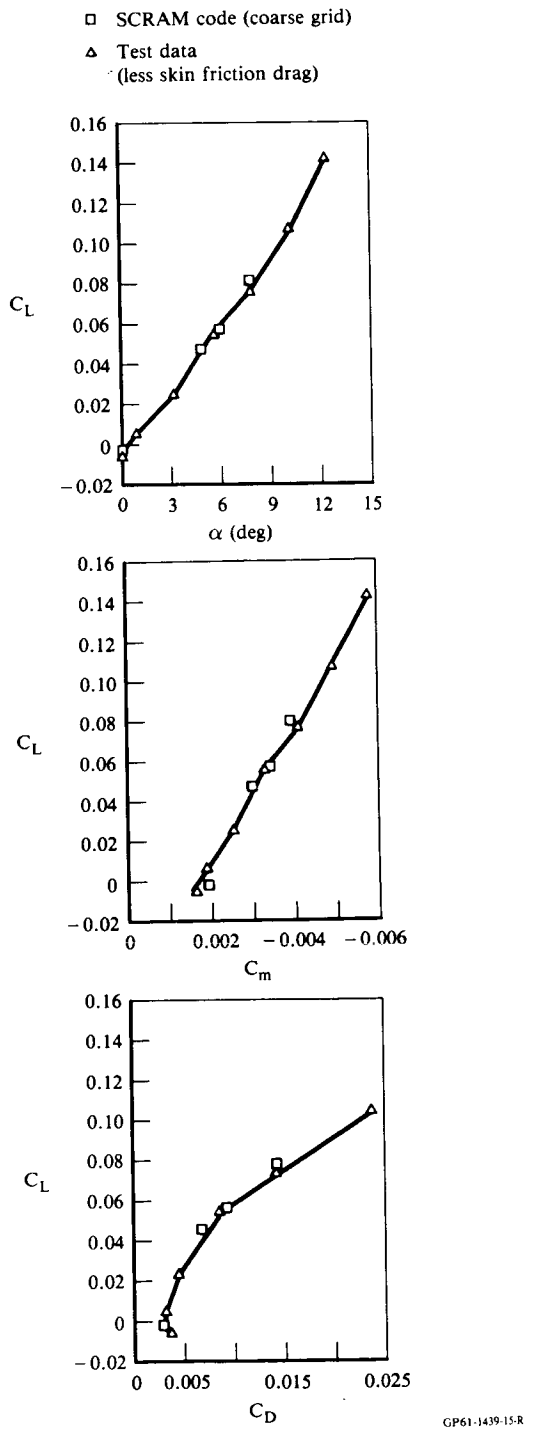

Fig. 14 SCRAM force and moment predictions for AMI-X blended body; $M_\infty = 6.0$.

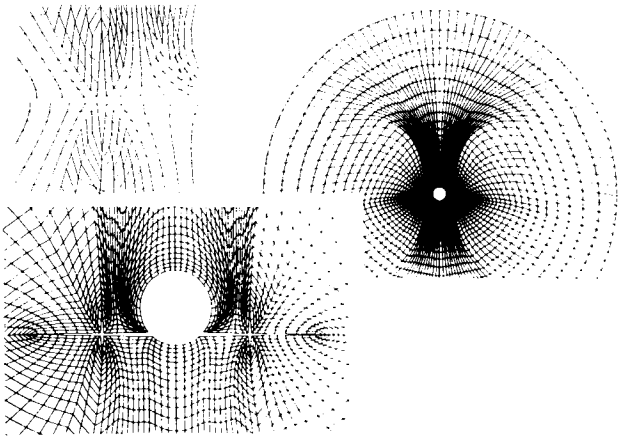

GP61-1439-16-R

Fig. 15 MARCHG grid generation for SCRAM code.

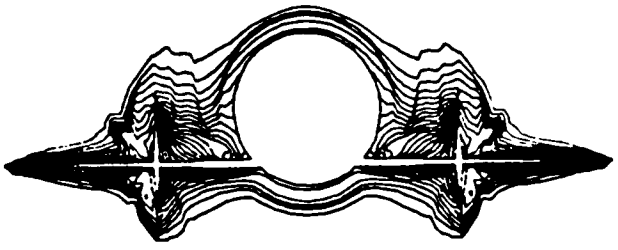

GP61-1439-17-R

Fig. 16 SCRAM code application to complex hypersonic vehicle; $M_\infty = 10$ and $\alpha = 0°$.

5. **Integrated Flowfield Analysis Methodology for Fighter Inlets** (R. R. Cosner, McDonnell Aircraft Company, St. Louis, MO)

A methodology to predict viscous flow over integrated fighter forebody-inlet combinations has been developed at McDonnell Aircraft Company; effects of Mach number, Reynolds number, angle of attack and engine mass flow are included in the prediction. A detailed description of the method is given by Cosner (1986), including the following examples.

The procedure is based on the velocity-splitting method which provides a relaxation solution to the steady-state Navier-Stokes equations [Cosner (1982)]. A multiple-zone mesh achieves the geometric flexibility required for representation of realistic inlet/forebody configurations. The mesh is generated by a three-dimensional implementation of Thompson's method, with wall orthogonality enhanced by a three-dimensional extension of Sorenson's technique, as described by Cosner (1982).

All terms, except time derivatives, were retained in the Navier-Stokes equations; turbulence effects were represented by the Cebeci-Smith algebraic model. Non-conservative and quasi-linearized discretization was used, and type-dependent differencing, according to the local flow velocity, ensured numerical stability without addition of artificial viscosity terms.

Separate mesh and flow solutions were executed in each of the three zones; the flow solutions are coupled by matching boundary conditions between adjacent zones during the iterative solution procedure. The mesh solutions were executed to a maximum of 30 iterations using an alternating-direction implicit scheme; formal convergence was not found to be necessary for achievement of a valid mesh.

The definition of the three computational zones is shown in figure 17. The external flowfield upstream and downstream of the inlet highlight comprises the forebody and centerbody zones, respectively; the internal zone extends from the inlet entrance to the throat or the engine face. Mesh parameters, such as node distribution or stretching coefficients in each coordinate direction can be prescribed entirely independently in each zone. The flow solution is coupled across the interface by interpolating Dirichlet and Neumann boundary condition data; mesh coordinates and dependent variables are modeled using piecewise bilinear functions. The flow solution algorithm selects the appropriate boundary condition according to the type of local flow in the adjoining zones at or near the interface.

The iterative solution procedure uses an alternating-direction implicit scheme. The cycle updates each zone in turn, starting with the forebody. In the internal zone, an algebraic correction to provide mass continuity in the potential field significantly enhances the rate of convergence. Typically, 10 to 30 solution cycles are required; a larger number is necessary when the free-stream Mach number approaches one from either direction or the viscous interactions are strong. Also, a modified procedure is used at near-choking conditions in the inlet.

Application of the zonal forebody-inlet code to the F/A-18 configuration used 8000 computational nodes (16x25x20) in the forebody zone, 4000 nodes (8x25x20) in the centerbody zone, and 6000 (12x25x20) in the inlet; the quasi-cylindrical mesh topology is shown in figure 18. Pressure distributions on the forebody in front of the inlet are shown in figure 19 at M=0.8 for three engine mass-flow rates from near-maximum to zero flow. The mass-flow rate variation was introduced into the computation only in the inlet zone, from which the perturbation propagated through the zone boundary into the forebody zone. As shown in Cosner (1986), especially good agreement with wind tunnel tests was obtained in the critical region inside the lower intake lip. The computations were performed on a CDC CYBER 176, typical times being 10 to 15 minutes.

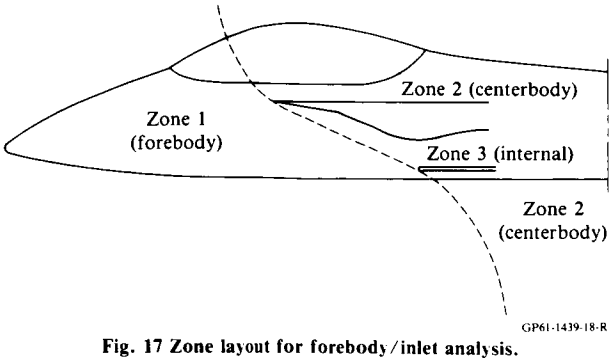

Fig. 17 Zone layout for forebody/inlet analysis.

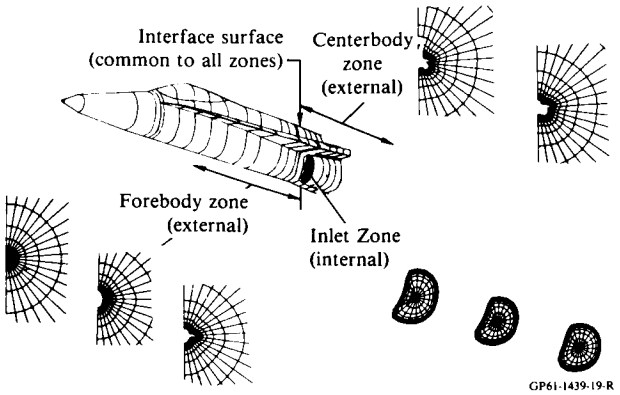

Fig. 18 Zonal mesh for F/A-18A forebody/inlet analysis.

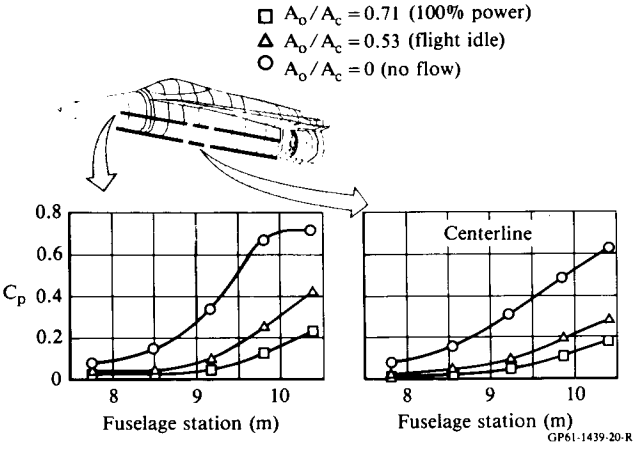

Fig. 19 Effect of engine airflow on F/A-18A forebody pressure; Mach = 0.8 and $\alpha = 0°$ (A_0 = inlet mass flow area, A_c = inlet capture area, corrected to free-stream conditions).

Figure 20 shows the three-zone mesh interfaces for an AV-8B forebody/inlet configuration; a total of 53760 nodes were used. Computations made on a Digital Equipment Corporation VAX 11/780 computer required 20 to 25 hours of wall-clock time. Computed surface-pressure distributions and comparison of the lower inlet lip inboard pressure with a test at M=0.9 are shown in figure 21. Figure 22 shows, for M=0.67, the inlet entrance flowfield from which detailed total and static pressure distributions in the inlet can be derived for design purposes.

The zonal procedure for solving the Navier-Stokes equations is being extended to integrated external compression inlets at all Mach numbers of interest, and to include the effects of wing and canard surfaces.

6. **Euler Calculations of a Helicopter Rotor in Hover and Forward Flight** (R. K. Agarwal and J. E. Deese, McDonnell Douglas Research Laboratories, St. Louis, MO).

The progressive increase of computing power over the last decade has advanced the computation of helicopter rotor flowfields from solution of transonic small-disturbance equations first to that of the full potential equations, and recently, to

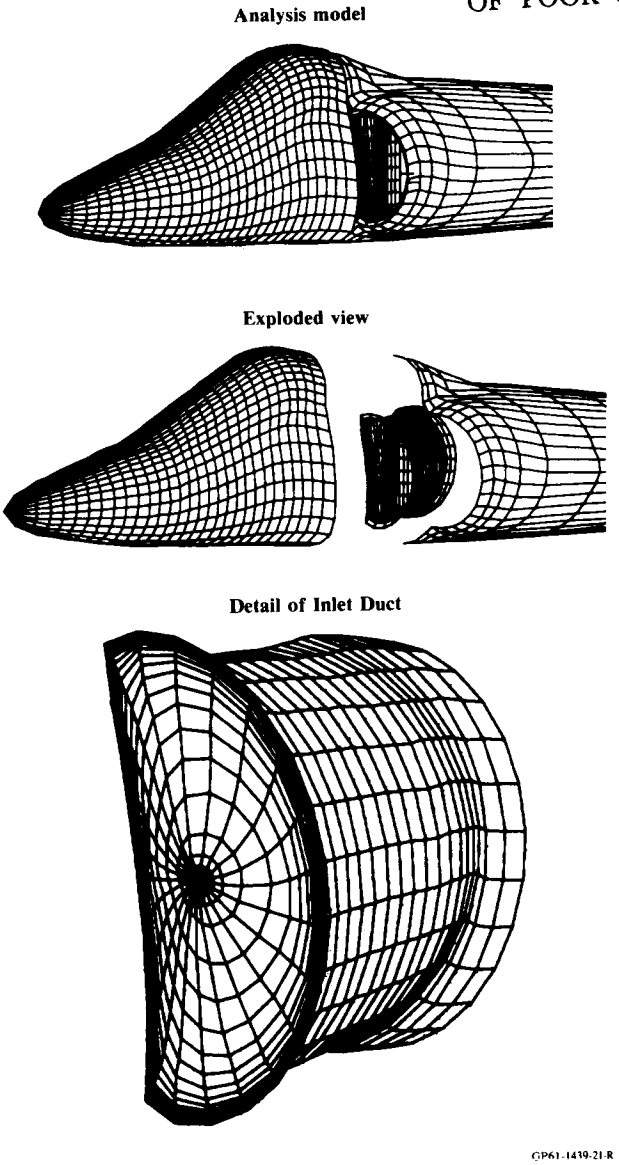

Fig. 20 Three-zone surface mesh for AV-8B forebody inlet.

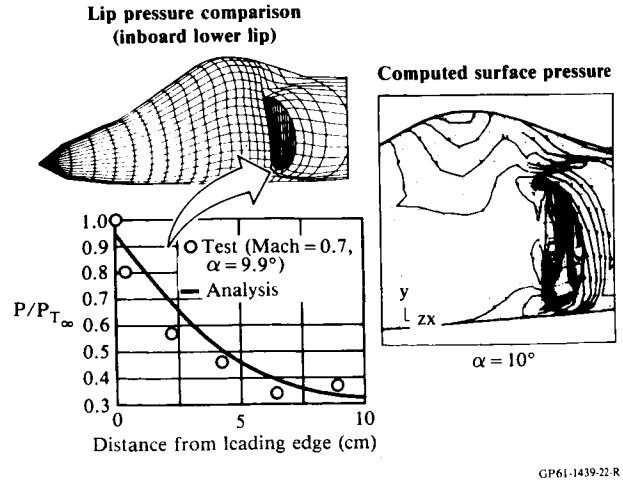

Fig. 21 AV-8B forebody inlet viscous analysis; Mach = 0.67, $\alpha = 10°$, and 186 kg/s (corrected).

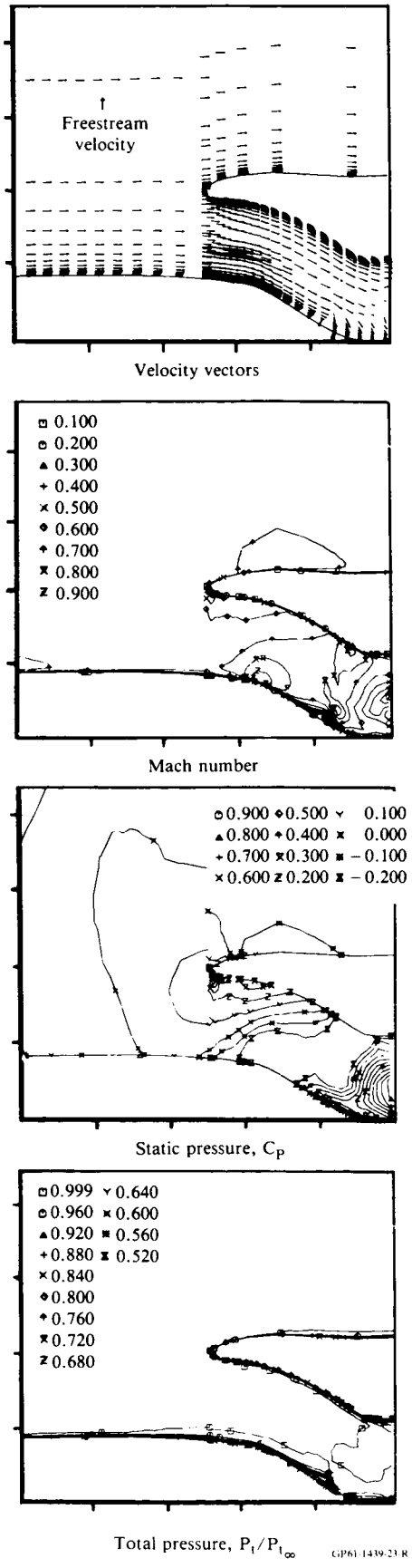

Fig. 22 AV-8B computed inlet entrance flowfield; Mach = 0.67, $\alpha = 0°$, and 186 kg/s.

codes based on the Euler equations. An Euler code, designated MDROTH, has been developed at the McDonnell Douglas Research Laboratories for calculating the flowfield of a multibladed helicopter rotor in hover and forward flight.

The code solves the three-dimensional Euler equations in a rotating coordinate system on body-conforming curvilinear grids around the blades. Euler equations are recast in absolute flow variables so that the absolute flow in the far field is uniform, but the relative flow is non-uniform. Equations are solved for the absolute flow variables by employing Jameson's finite-volume explicit Runge-Kutta time-stepping scheme. Rotor wake effects are modeled in the form of a correction applied to the geometric angle-of-attack along the blades. This correction is obtained by computing the local induced downwash with a free-wake analysis program. The details of the methodology are described by Agarwal and Deese (1986).

A set of test calculations was performed by Agarwal and Deese* to verify the code for a model rotor in hover and forward flight at various collective pitch angles. The model rotor has two untwisted, untapered blades of aspect ratio equal to six and the NACA 0012 airfoil section. Computations were performed on a 97 (chordwise) x 33 (blade-normal) x 21 (spanwise) mesh.

The code has been fully vectorized for optimum performance on Cray X-MP, and has also been microtasked for peak performance on the four-processor Cray X-MP/48 [Booth and Misegades (1986)] with a speed-up factor of 3.71. A typical case requires 2 million 64-bit words of main memory and 7×10^{-6} seconds of CPU time per mesh point for each iteration. A solution for hover flowfield converged in 500 to 800 iterations. This project has been accepted for access to the NAS Cray-2.

Figure 23 shows the main features of the flowfield of a two-bladed rotor in hover, with the imbedded finite-difference grid and the coordinate system. The flowfield is characterized by transonic shocks, complex vortical wakes, and blade-vortex interactions.

Comparisons of computed pressure distributions with experimental data are shown in figure 24 for a hovering rotor at a tip Mach number of M_t=0.52 and zero collective pitch, and for M_t=0.877 and collective pitch angle θ_c=8° in figure 25. Both cases indicate good agreement; in the lifting case of figure 25, further improvement can be achieved by refining the wake model.

For forward flight, computed pressure distributions are compared with experimental data at a location near the blade tip in figure 26 for M_t=0.8, advance ratio μ=0.2, and zero collective pitch. Again, good agreement is demonstrated.

The long-term objective of this project is to include viscous effects in the calculation of transonic multibladed rotor flowfields.

*Agarwal, R. K. and Deese, J. E., "An Euler Solver for Calculating the Flowfield of a Helicopter Rotor in Hover and Forward Flight," McDonnell Research Laboratories, St. Louis, MO, 1987.

7. **Transonic Wing/Body Calculations Using the Slender-Layer Navier-Stokes Approximation** (R. K. Agarwal and J. E. Deese, McDonnell Douglas Research Laboratories, St. Louis, MO)

With the increasing availability of supercomputers, the ability to compute transonic flowfields has progressed to solution of Reynolds-averaged Navier-Stokes equations for aircraft configurations. A viscous flow code, designated MDSSL30, has been developed at McDonnell Douglas Research Laboratories for calculation of transonic wing/body flowfields.

The code computes the turbulent flowfield by solving the three-dimensional, Reynolds-averaged, slender-layer approximation to the Navier-Stokes equations on body-conforming, curvilinear grids. In the slender-layer approximation to the Navier-Stokes equations, only streamwise diffusion terms are neglected; diffusion terms in the other directions are retained. Therefore, slender-layer equations are suitable for calculating spanwise separation and the flow along a wing-body junction. These equations are solved by employing Jameson's finite-volume explicit Runge-Kutta time-stepping scheme. The calculations performed so far have used the Baldwin-Lomax turbulence model.

The details of the methodology and the test calculations performed to verify the code are described by Agarwal, Deese, and Underwood (1985) and Agarwal and Deese (1984). Recently, fine-grid calculations for turbulent flow over an ONERA-M6 wing were performed on a Cray X-MP/48; the code was fully optimized and microtasked for peak performance on the four-processor Cray X-MP/48, as documented by Booth and Misegades (1986).

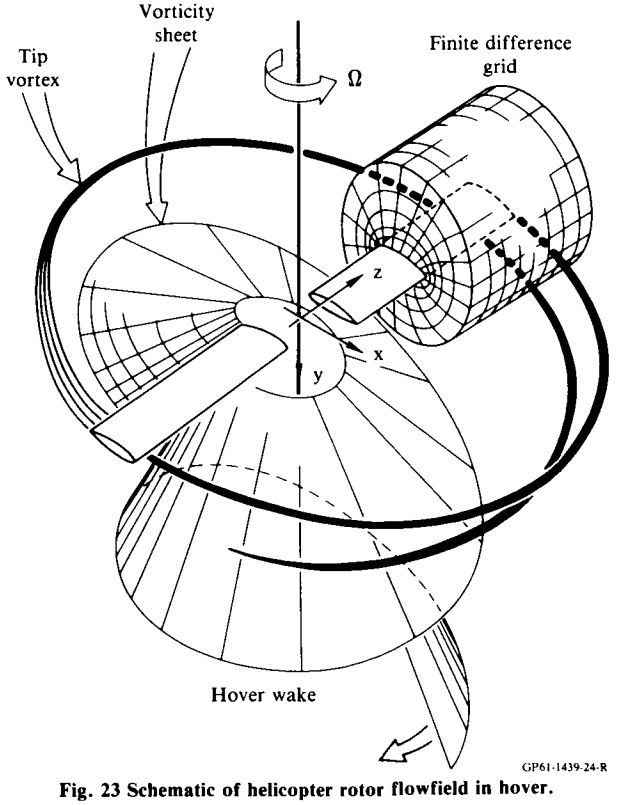

Fig. 23 Schematic of helicopter rotor flowfield in hover.

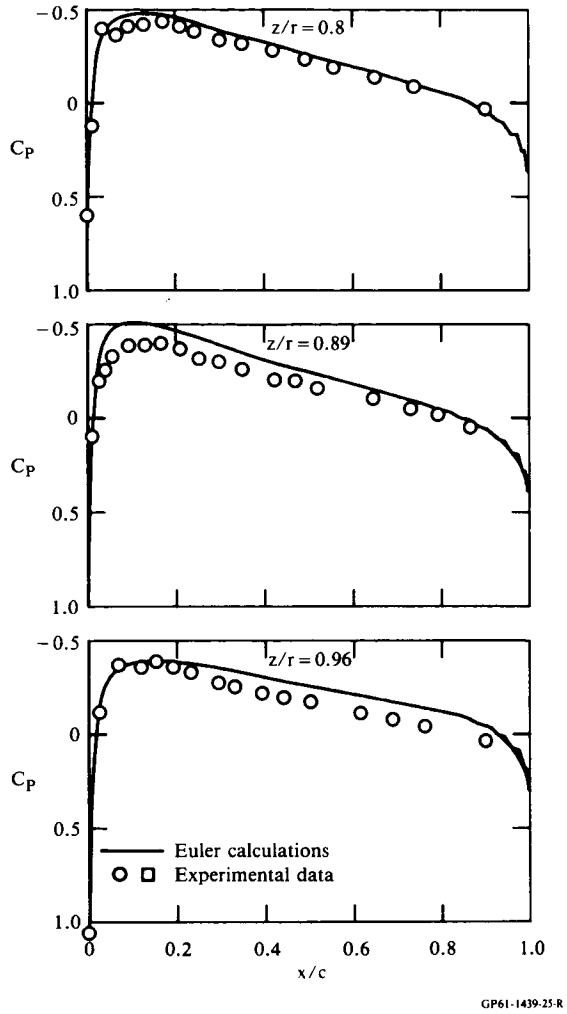

Fig. 24 Surface pressure distributions on a nonlifting rotor in hover; $M_t = 0.52$, $\theta_c = 0°$, AR = 6, NACA 0012 blade, and $97 \times 33 \times 21$ mesh.

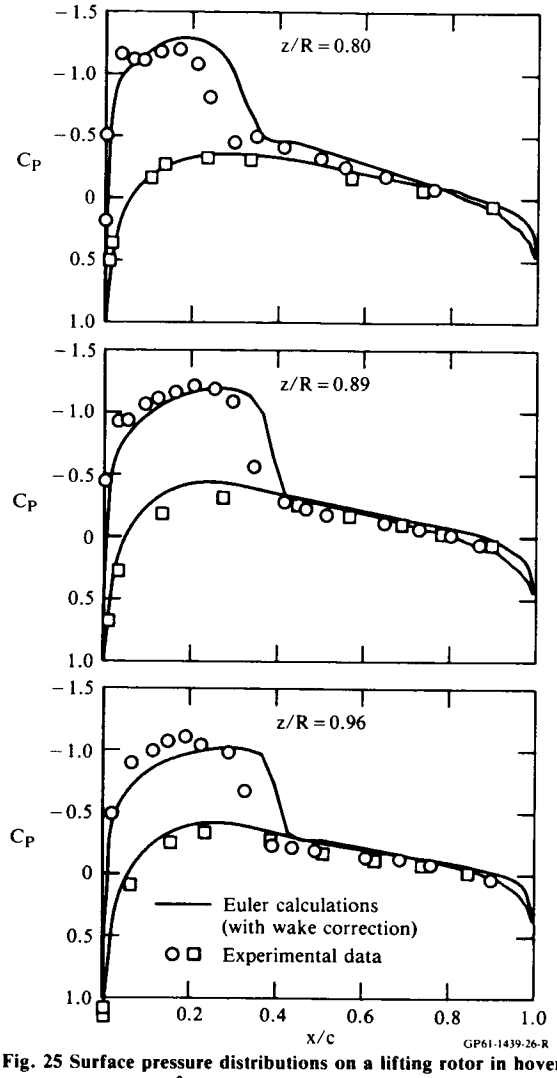

Fig. 25 Surface pressure distributions on a lifting rotor in hover; $M_t = 0.877$, $\theta_c = 8°$, AR = 6.0, NACA 0012 blade, and $97 \times 33 \times 21$ mesh.

Computed results at various spanwise stations of the ONERA-M6 wing are compared with experimental data in figure 27, with good agreement. The code has also been exercised by Deese and Agarwal* for calculation of fighter- and transport-type wing/body flowfields; excellent global grids were generated with the three-dimensional procedure of Chen, Vassberg, and Peavey (1985). Surface grid-lines of a transport wing/body configuration are shown in figure 28. Comparisons of calculated pressure distributions at various spanwise stations with experimental data are shown in figure 29; the agreement is again good.

The long-term objective of this project is to calculate turbulent flowfields for increasingly complete transport and fighter aircraft configurations. The project has also been accepted for access to the NAS Cray-2.

8. Concluding Remarks

An extensive program to develop advanced CFD codes is being conducted within the components of the McDonnell Douglas Corporation for applications to helicopters, transport and fighter aircraft, and missiles and hypersonic vehicles. Efficient use of large computers, including multiple-processor facilities, is receiving special attention, and access to the NAS facility in several of these areas is greatly appreciated.

*Deese, J. E. and Agarwal, R. K., "Navier-Stokes Calculations of Transonic Viscous Flow About Wing-Body Configurations," McDonnell Douglas Research Laboratories, St. Louis, MO, 1987.

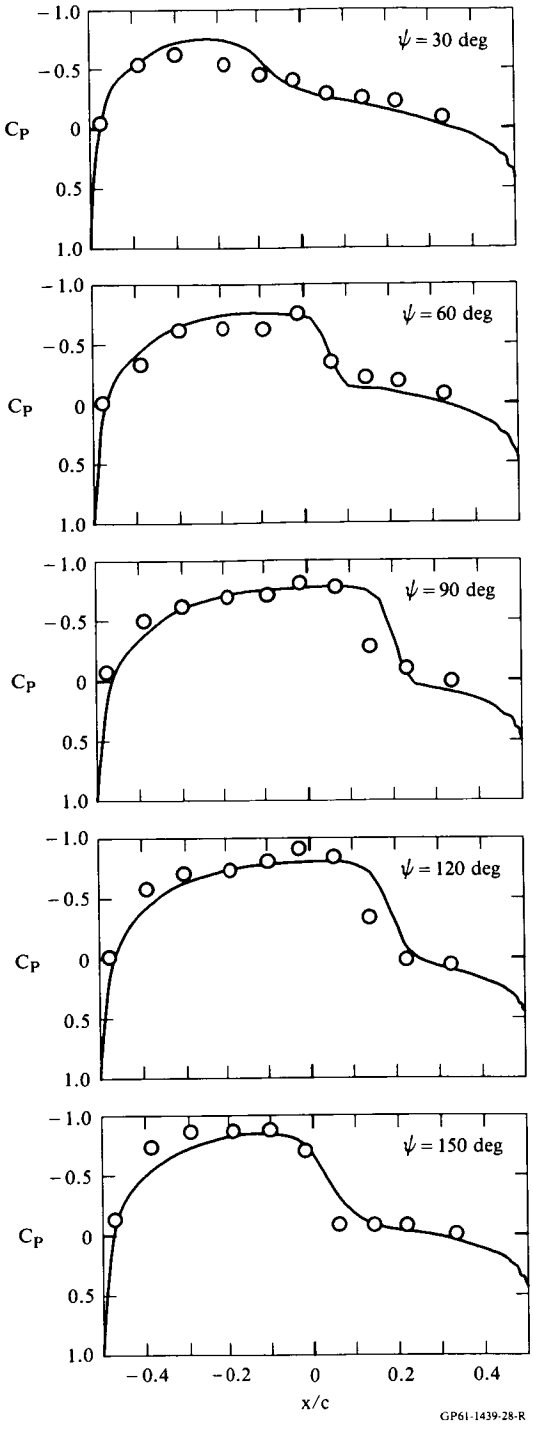

Fig. 26 Euler calculations for flowfield of a helicopter rotor in forward flight; $M_t = 0.8$, $\mu = 0.2$, and $96 \times 32 \times 32$ mesh.

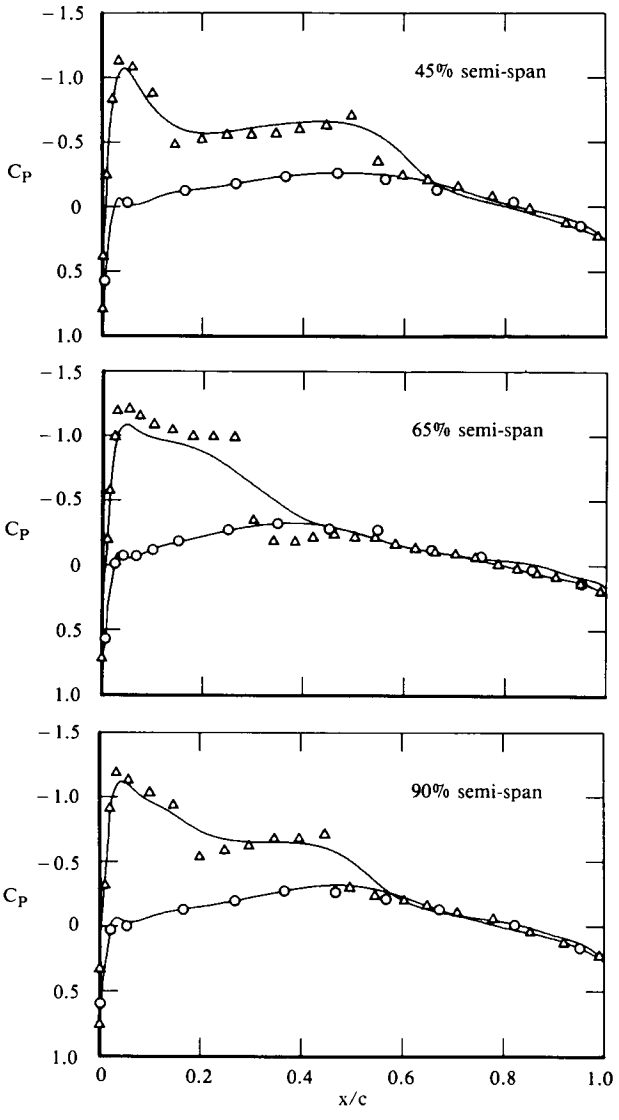

Fig. 27 Transonic viscous wing calculations on CRAY X-MP/48 for the ONERA-M6 wing; $M_\infty = 0.84$, $\alpha = 3.06°$, $Re_c = 11.72 \times 10^6$, and $140 \times 48 \times 32$ mesh.

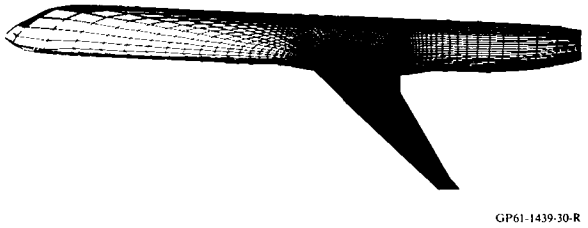

Fig. 28 Grid lines on the surface of a transport wing-body configuration.

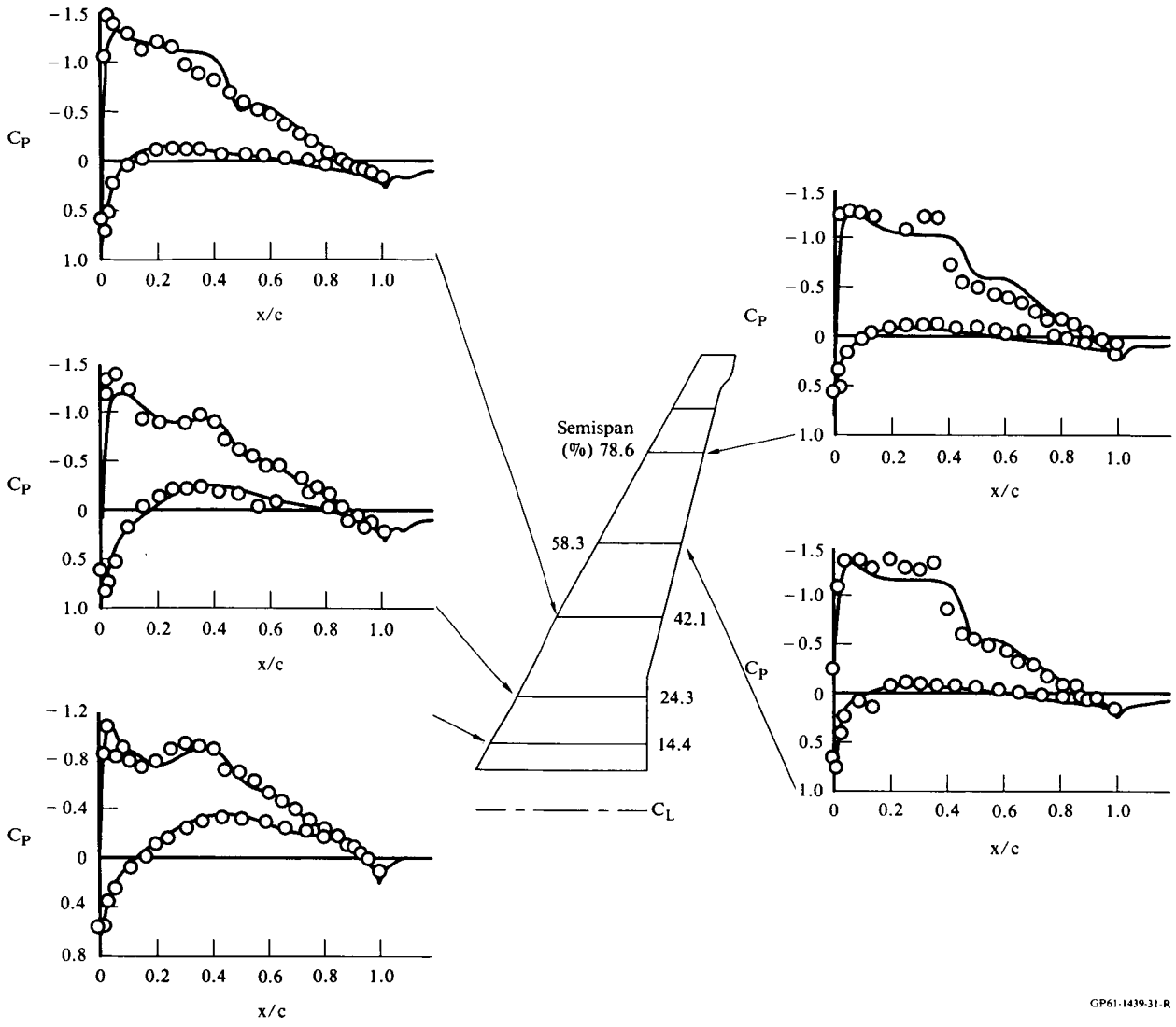

Fig. 29 Navier-Stokes solutions for flow past a transport-type wing-body; $M_\infty = 0.76$, Re = 6.39 million, $\alpha = 2°$.

REFERENCES:

Agarwal, R. K.; and Deese, J. E.: Computation of Viscous Airfoil, Inlet, and Wing Flowfield. AIAA 84-1551, 1984.

Agarwal, R. K.; and Deese, J. E.: Euler Calculations for Flowfield of a Helicopter Rotor in Hover. AIAA 86-1782CP, 1986.

Agarwal, R. K.; Deese, J. E.; and Underwood, R. R.: Computation of Transonic Viscous Wing-Body Flowfields Using Unsteady Parabolized Navier-Stokes Equations. AIAA 85-1595, 1985.

Booth, M.; and Misegades, K.: Microtasking: A New Way to Harness Multiprocessors. Cray Channels, Vol. 8, No. 2, Summer 1986, pp. 24-27.

Cebeci, T.; Clark, R. W.; Chang, K. C.; Halsey, N. D.; and Lee, K.: Airfoils with Separation and the Resulting Wakes. J. of Fluid Mechanics, Vol. 163, 1986, pp. 323-347.

Chen, L. T.; Li, S.; and Chen, H.: Calculation of Transonic Airfoil Flows by Interaction of Euler and Boundary-Layer Equations. AIAA 87-521, 1987.

Chen, L. T.; Vassberg, J. C.; and Peavey, C. C.: A Transonic Wing/Body Flowfield Calculation with Improved Grid Topology. AIAA J., Vol. 23, Dec. 1985, p. 1877-1884.

Cosner, R. R.: Relaxation Solution for Viscous Transonic Flow about Fighter-Type Forebodies and Afterbodies. AIAA 82-0252, 1982.

Cosner, R. R.: Integrated Flowfield Analysis Methodology for Fighter Inlets. AIAA 86-1463, 1986.

Gregg, R. D.; and Misegades, K.: Transonic Wing Optimization Using Evolution Theory. AIAA 87-0520, 1987.

Verhoff, A.; and O'Neil, P. J.: A Natural Formulation for Numerical Solution of the Euler Equations. AIAA 84-0163, 1984.